Redshift of light emitted by particles orbiting a black hole immersed in a strong magnetic field

L.A. López[1] · **Nora Breton**[2]

Abstract In this paper we analyze the frequency shifts of the light emitted by particles describing stable circular geodesics around a static black hole immersed in an external magnetic field of arbitrary strength. This system is represented by the Ernst solution of the Einstein-Maxwell equations. The presence of the magnetic field and its magnitude affects both the geodesics and the red-blueshifts of the light emitted by neutral or charged particles orbiting the black hole. When the magnetic field is turned off we recover the characteristic redshifts coming from particles orbiting a Schwarzschild black hole.

1 Introduction

Astrophysical objects such as black holes have been of great interest to the scientific community for many years; this interest has increased even more due to the possibility of observing strong field gravitational phenomena. For example the analysis of black hole stability played and outmost role in characterizing gravitational-wave signals detected (Abbott et al. 2016). The project GRAVITY (Eisenhauer

✉ L.A. López
lalopez@uaeh.edu.mx

N. Breton
nora@fis.cinvestav.mx

1 Área Académica de Matemáticas y Física., UAEH, carretera Pachuca-Tulancingo km 4.5, C.P. 42184, Mineral de la Reforma, Hidalgo, Mexico

2 Departamento de Física, Centro de Investigación y de Estudios Avanzados del I.P.N, Cinvestav, A.P. 14-740, Mexico City, Mexico

et al. 2009) tracks the stars orbiting around the supermassive black hole at the center of our galaxy and the Event Horizon Telescope (EHT) collaboration was able to obtain an image of the supermassive black hole in M87* (Akiyama et al. 2019), which opens the way for a phenomenological approach for a deeper understanding of Black Holes (BH). Therefore, it is necessary to study the relationship between the observed gravitational phenomena and the parameters that characterize BH, such as the mass, angular momentum or charge. In this sense in (Cardoso et al. 2009) was shown the relationship among parameters of the circular null geodesics, Lyapunov exponents, and quasinormal modes of black holes (BH). In this context, different BH solutions have been studied (Fernando and Correa 2012) (Breton and Lopez 2016) (Lopez and Hinojosa 2021). In (Konoplya and Stuchlík 2017) the limits of applicability of this correspondence were addressed.

Also in (Herrera-Aguilar and Nucamendi 2015) the authors developed a theoretical approach to obtain the parameters of a Kerr BH in terms of the redshift and blueshift of photons emitted by particles traveling along stable circular geodesics. Using this idea, different configurations have been studied; in (Becerril et al. 2016), were derived the red/blueshifts of static spherically symmetric BH and in (Kraniotis 2021) were studied the red/blueshifts and frame dragging of the Kerr–Newman–de Sitter and Kerr–Newman BH.

On the other hand, observational evidence indicates that in the center of each galaxy there are black holes (Begelman 2003) and always accompanied by magnetic fields whose origin may be external or generated by currents in the accretion disk.

The Ernst solution (Ernst 1976) of the coupled Einstein-Maxwell equations describes the gravity of a static black hole immersed in a uniform magnetic field; it is also known

as Schwarzschild–Melvin (SM) BH. Despite being non asymptotically flat, the magnetic Ernst solution is a useful model for a black hole in certain astrophysical situations. For charged particles geodesics of the Ernst BH have been described in (Dadhich et al. 1979) as well as for Melvin Universe (magnetic universe), obtaining that for charged particles bound orbits always exist for realistic magnetic field strengths.

Frequently it has been considered the external magnetic field as a perturbation or test field (test field approximation); for instance, the Wald (Wald 1974) solution consists in a test magnetic field that does not affect the curvature. This solution has been addressed in (Frolov and Shoom 2010), where the bounded trajectories of charged particles near a weakly magnetized Schwarzschild BH were derived; in this setting neutral particles are not affected by the presence of the weak magnetic field. In (Lim 2015) is studied the influence of an external uniform electric or magnetic field on charged particles via the Lorentz interaction. In (Tursunov et al. 2016) the analysis of circular orbits and related quasi-harmonic oscillatory motion of charged particles around weakly magnetized rotating black holes was addressed. In (Hackstein and Hackmann 2020) were studied the Innermost Stable Circular Orbits (ISCOs) of charged particles in a weak electromagnetic field in the vicinity of a Schwarzschild BH.

In (Aliev and Ozdemir 2002) the motion of charged particles around a rotating BH in a weak magnetic field was analyzed, obtaining that the presence of the magnetic field enlarges the region of marginal stability shifting the radius of the marginal stable orbits towards the horizon. In (Konoplya 2007) corrections to the bending angle and time delay due-to presence of weak magnetic fields in galaxies were estimated.

As was briefly summarized, charged particles trajectories have been thoroughly studied in the spacetime of a BH in a weak magnetic field. Most of the treatments apply to test magnetic fields that do not alter curvature, therefore it has not effect on uncharged or neutral particles. The advantage of studying an exact solution of the Einstein-Maxwell equations is that the magnitude of the magnetic field is arbitrary and, as we show in the following, acting through curvature it has an effect even on neutral test particles, enlarging as well the region of stable circular orbits by pushing the ISCO orbits towards the horizon.

In this work our aim is to determine the redshift of the light emitted by particles orbiting the Ernst BH in stable circular trajectories; therefore we focus on these kind of orbits for both, charged and uncharged test particles, pointing out that the latter are indeed influenced by the magnetic field even if it is not too strong; we present as well the region of the ISCO, in terms of the dimensionless parameter mB (m the BH mass and B the magnetic field). Moreover, we determine the upper bound on mB that allows stable circular

orbits. Then is determined the influence of the external magnetic field on the redshifts coming from particles (charged or uncharged) orbiting in stable circular trajectories around the Ernst BH.

The paper is organized as follows: in Sect. 2 the Ernst or Schwarzschild–Melvin (SM) BH is introduced as well as the effective potentials for charged and uncharged particles. In Sect. 3 a short summary is given to determine the frequency shifts of photons emitted from particles moving in stable geodesics around a static BH. Also the frequency shifts of light emitted by neutral and charged particles orbiting the Ernst BH are determined. Finally, conclusions are given in the last section.

2 The Ernst or Schwarzschild-Melvin black hole

The Ernst solution or Schwarzschild–Melvin (SM) BH, also known as electrified/magnetized Schwarzschild BH, describes the spacetime of a static BH immersed in an external uniform magnetic or electric field; in spherical coordinates the metric is described by (Ernst 1976),

$$ds^2 = \Lambda^2(-\Delta dt^2 + \Delta^{-1}dr^2 + r^2 d\theta^2) + \Lambda^{-2}r^2\sin^2\theta d\phi^2,$$

(1)

with $\Lambda = 1 + \frac{1}{4}B^2 r^2 \sin^2\theta$ and $\Delta = 1 - \frac{2m}{r}$, where m is the BH mass and B is the external magnetic field parameter. As was shown in (Wild and Kerns 1980) where the Gaussian curvature was examined, the event horizon remains the same as for Schwarzschild, located at $r = 2m$ and the curvature singularity at $r = 0$. When $m \to 0$ the metric reduces to the Melvin's magnetic universe (Melvin 1965).

It is worth to note that the effect of the magnetic field resembles the one of a cosmological constant: writing the tt metric component (with $\theta = \pi/2$, just for simplicity),

$$g_{tt} = -\Delta\Lambda^2 = -\left(1 + \frac{B^2 r^2}{2} + \frac{B^4 r^4}{16} - \frac{2m}{r}\Lambda^2\right),$$

(2)

the second term with dependence on r^2 acts similarly to a positive cosmological constant, from which we can guess the confining effect that the magnetic field exerts on test particles as well as on light. Also due to the presence of the electromagnetic field, the metric (1) is not asymptotically flat.

The vector potential $A_\mu = (A_t, 0, 0, A_\phi)$, for an electric field $\mathcal{E}$ and magnetic field B, is given by (Lim 2015), (Konoplya and Fontana 2008),

$$A_t = \mathcal{E}r\Delta\Lambda\cos\theta, \quad A_\phi = \frac{1}{2\Lambda}Br^2\sin^2\theta.$$

(3)

In the context of astrophysics typically magnetic fields are considered in the test field regime, that do not influence the spacetime curvature. In that case the metric is simply the Schwarzschild metric ($\Lambda = 1$ in (1)) with the magnetic field associated to A_ϕ.

2.1 Effective potential for a charged test particle

The equations of motion of a charged particle with mass m_c and charge q_c may be derived from the Lagrangian;

$$\mathcal{L} = \frac{1}{2} g_{\mu\nu} \dot{x}^\nu \dot{x}^\mu + \kappa A_\mu \dot{x}^\mu, \tag{4}$$

where $\kappa = q_c/m_c$ is the specific charge of the test particle and A_μ is the electromagnetic potential.

The momenta conjugate is given by

$$P_\mu = g_{\mu\nu} \dot{x}^\nu + \kappa A_\mu. \tag{5}$$

For axisymmetric stationary spacetimes a test particle has two conserved quantities, its energy and its angular momentum, related to the two Killing vectors ∂_t and ∂_ϕ, respectively,

$$P_t = g_{tt}\dot{t} + \kappa A_t = g_{tt}U^t + \kappa A_t = -E, \tag{6}$$

and

$$P_\phi = g_{\phi\phi}\dot{\phi} + \kappa A_\phi = g_{\phi\phi}U^\phi + \kappa A_\phi = L. \tag{7}$$

The components of the 4-velocity of the test particle are $U^t = -(E + \kappa A_t)/g_{tt}$ and $U^\phi = (L - \kappa A_\phi)/g_{\phi\phi}$. If the 4-velocity is normalized to unity $U^\mu U_\mu = -1 = g_{tt}(U^t)^2 + g_{rr}(U^r)^2 + g_{\theta\theta}(U^\theta)^2 + g_{\phi\phi}(U^\phi)^2$ then we obtain;

$$-1 = \frac{(E + \kappa A_t)^2}{g_{tt}} + g_{rr}\dot{r}^2 + \frac{(L - \kappa A_\phi)^2}{g_{\phi\phi}} + g_{\theta\theta}\dot{\theta}^2. \tag{8}$$

Comparing with $g_{rr}\dot{r}^2 + V_{\text{eff}} = 0$ we get the effective potential over the test particle, which depends on E and L,

$$V_{\text{eff}} = 1 + \frac{(E + \kappa A_t)^2}{g_{tt}} + \frac{(L - \kappa A_\phi)^2}{g_{\phi\phi}}. \tag{9}$$

We shall consider only magnetic field, i.e. $\mathcal{E} = 0$, $A_t = 0$; for equatorial orbits $\theta = \pi/2$ and using (1) and the vector potential for the magnetic field (3) we obtain that

$$V_{\text{eff}} = 1 - \frac{E^2}{\Delta\Lambda^2} + \frac{\Lambda^2}{r^2}\left(L - \kappa\frac{Br^2}{2\Lambda}\right)^2. \tag{10}$$

In Fig. 1a) is shown the behavior of V_{eff}, Eq. (10), for different values of the specific charge κ and Fig. 1b) shows V_{eff} for different values of the dimensionless parameter mB. The
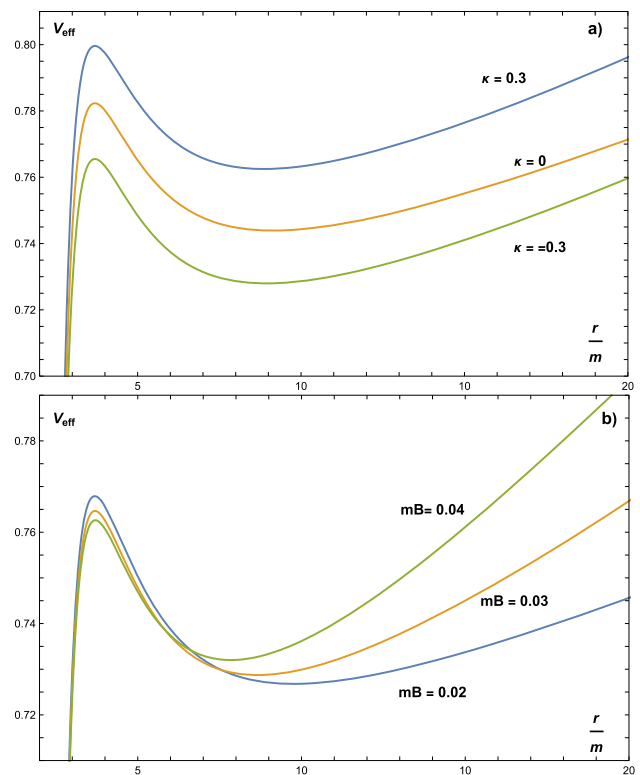

Fig. 1 **a)** The behavior of the effective potential V_{eff} for different values of the specific charge of the test particle, κ, with $E = 0.5$, $\frac{L}{m} = 2.1$ and $mB = 0.027$. **b)** The behavior of the effective potential V_{eff} varying mB with $\frac{L}{m} = 2.1$, $E = 0.5$ and $\kappa = 0.3$ The effect of the magnetic field is of confining, even for uncharged test particles ($\kappa = 0$)

effective potential presents maximum and minimum that indicates there exist circular orbits, both, unstable and stable.

Therefore when considering a charged particle with mass m_c and charge q_c, the effect of the effective potential depends on the magnitude and sign of the specific charge κ. When mB increases, the confining effect increases, as can be seen in Fig. 1b).

When we consider the equation for radial motion $g_{rr}\dot{r}^2 + V_{\text{eff}} = 0$, the circular orbits correspond to the radii r_c, where the potential and its derivative are zero ($V_{\text{eff}}(r_c) = 0$ and $V_{\text{eff}}'(r_c) = 0$). Then for circular orbits, from Eq. (10) the following expression, that restricts L, should be fulfilled

$$\left(L - \kappa A_\phi\right)^2 a(r_c) + \left(L - \kappa A_\phi\right), b(r_c) + c(r_c) = 0 \tag{11}$$

where;

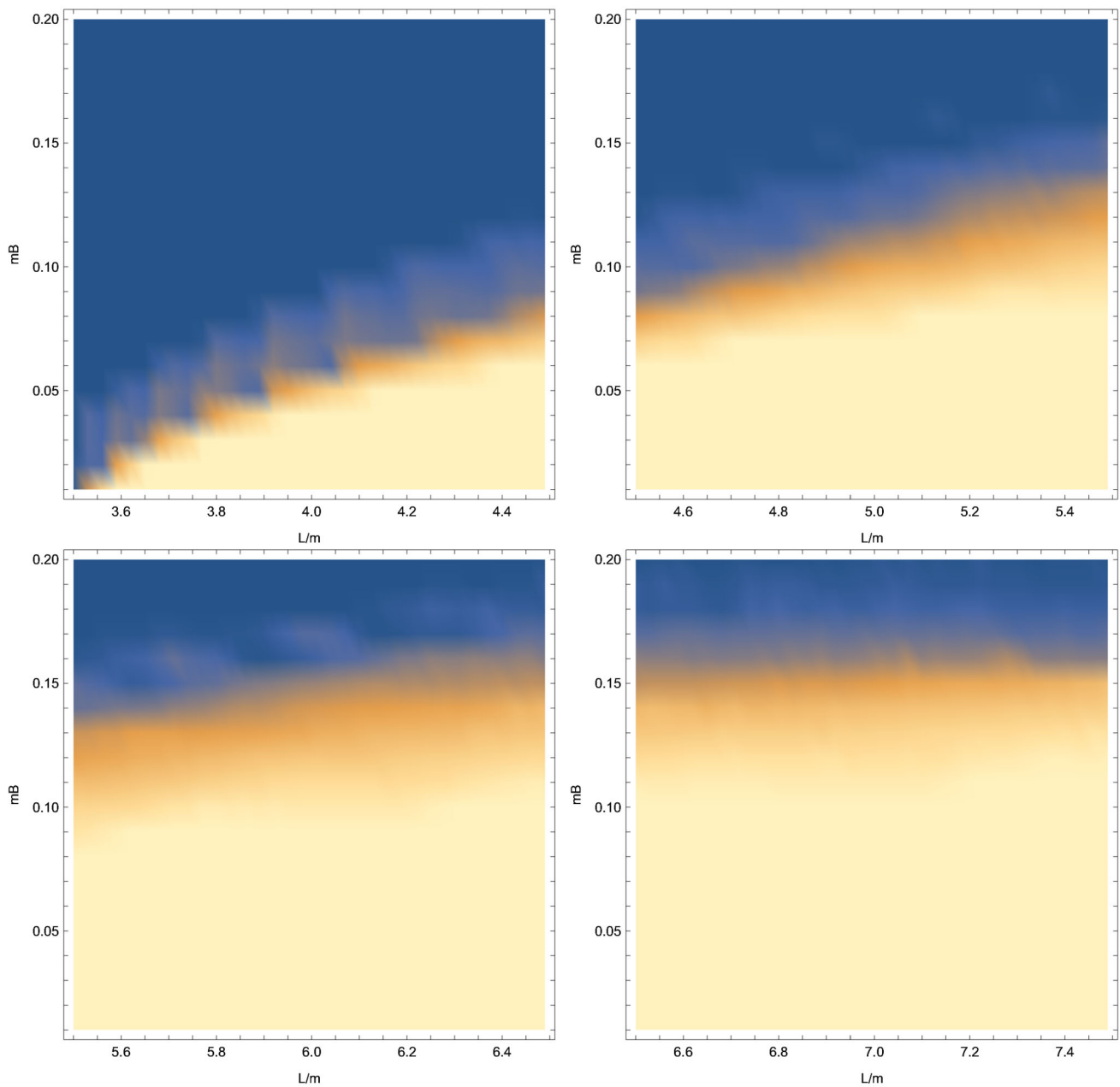$$a(r_c) = \frac{(4 + B^2 r^2)}{8(r - 2m)r^3}[B^2 r^2(3r - 5m) - 4(r - 3m)], \tag{12}$$

Fig. 2 Density plots for the parameters mB and L/m; the lighter regions correspond to the pairs $(L/m, B)$ of the stable circular orbits of the Ernst BH; the ranges are $0 \leq mB \leq 0.2$ and $0 \leq \kappa \leq 1$

$$b(r_c) = \frac{4B\kappa}{r}, \quad c(r_c) = \frac{2[4m + B^2r^2(2r - 3m)]}{r(r - 2m)(4 + B^2r^2)}. \quad (13)$$

Moreover, the stability of the circular orbits requires that $V_{\text{eff}}''(r_c) > 0$. This analysis is performed numerically in the range of mB shown in Fig. 2; the density plots for the pairs $(L/m, mB)$ correspond to the stable circular orbits; in the ranges $0 \leq mB \leq 0.2$ and $0 \leq \kappa \leq 1$ a large number of stable circular orbits (represented by the lighter part of the graphs) is allowed.

2.2 Uncharged particles

The effective potential, Eq. (10), acting on uncharged test particles, $\kappa = 0$ is given by

$$V_{\text{eff}} = 1 - \frac{16rE^2}{(r - 2m)(4 + B^2r^2)^2} + \frac{L^2}{16r^2}\left(4 + B^2r^2\right)^2. \quad (14)$$
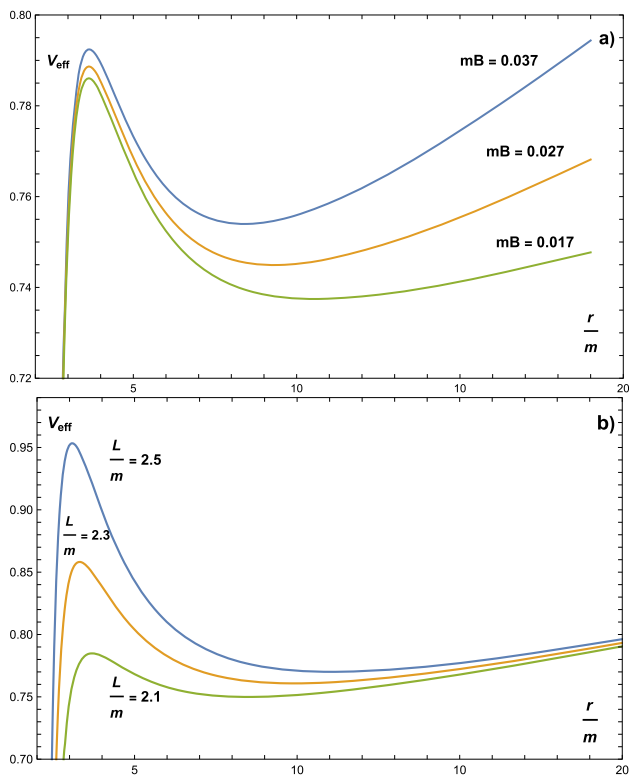
Fig. 3 **a)** For uncharged test particles, the effective potential as a function of r/m is plotted for different values of mB with $E = 0.5$ and $\frac{L}{m} = 2.1$. **b)**. The same for different values of $\frac{L}{m}$ with $E = 0.5$ and $mB = 0.034$

As shown in Fig. 3 the effective potential V_{eff} presents maximum and minimum, corresponding to circular orbits, unstable and stable, respectively. In Fig. 3a) V_{eff} (14) is shown as a function of r/m for different values of mB and in Fig. 3b) for different values of L/m. These plots show that uncharged particles are affected by the presence of the external magnetic field, even if it is not too strong, fact that has been disregarded in most of the literature.

If mB increases then the confining effect increases (see Fig. 3a)). The same happens when L/m increases (see Fig. 3b)) and the maxima of the effective potential is shifted towards the horizon, the effect is the opposite in the minima.

For the circular orbits the values of the energy and angular momentum of the test uncharged particle in terms of the BH parameters (m, B) are,

$$E^2 \big|_{r_c} = \frac{(r - 2m)^2(4 - r^2B^2)(r^2B^2 + 4)^2}{16r[4(r - 3m) - B^2r^2(3r - 5m)]}, \quad (15)$$

$$L^2 \big|_{r_c} = \frac{16r^2[B^2r^2(2r - 3m) + 4m]}{(4 + B^2r^2)^2[4(r - 3m) - B^2r^2(3r - 5m)]}, \quad (16)$$

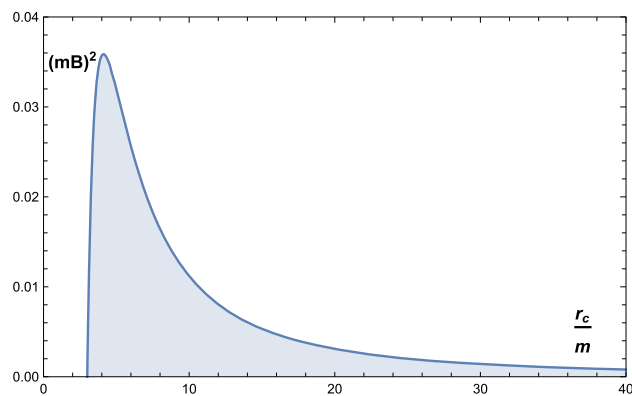evaluated at r_c, the radius of the circular orbit.

Fig. 4 The shaded region corresponds to the pairs (r_c, mB) that define a circular orbit. For values $Bm > 0.189366$, the maximum (not shown in the plot), no circular orbits occur

The conditions $0 \leqslant E^2$ and $0 \leqslant L^2$ at $r = r_c$ lead to the following constrictions between m, B and r_c:

$$B^2 < \frac{4(r_c - 3m)}{r_c^2(3r_c - 5m)}, \quad 3m \leqslant r_c. \quad (17)$$

The second condition is no other than r_c should be larger than the one corresponding to the photosphere radius for Schwarzschild, $r_{ph}^S = 3m$. The condition that r_c corresponds to a circular orbit that is stable is that the second derivative of the effective potential be positive, $V_{\text{eff}}''(r_c) > 0$. In Fig. 4 is shown the region of pairs $(r_c/m, (mB)^2)$ that correspond to circular orbits. As mB decreases the range of r_c/m augments; mB presents a maximum at $mB = 0.189366$, this means that for fields such that $mB > 0.189366$ no circular orbits occur. As mB grows the available range for r_c/m is shorter.

As shown in Fig. 4, the larger number of circular orbits is for values of mB well below the maximum $(mB)_{\text{max}} = 0.189366$. For concreteness we include Table 1 with the orders of magnitude of the parameter mB and the corresponding BH masses in solar mass units and the magnetic field B_{SI} in Tesla. To obtain the magnetic field in inverse length units, we use the factor $\sqrt{G\epsilon_0}/c^2$, where G is the gravitational constant and ϵ_0 is the vacuum dielectic contant; and M, the BH mass, given in Kg. is transformed to length units with $m = GM/c^2$. The maximum $(mB)_{\text{max}} = 0.189366$ could correspond to a ten solar mass BH with a magnetic field of $B_{\text{SI}} \approx 10^{16}$ Tesla (that is huge), or to a more massive BH in a less intense magnetic field.

The condition $V_{\text{eff}}''(r_c) > 0$ (stable circular orbits) sets additional bounds on the range of B already restricted by (17),

$$V_{\text{eff}}''(r_c) = 2\frac{\{y^3A_3(\tilde{m}) + y^2A_2(\tilde{m}) + yA_1(\tilde{m}) + A_0(\tilde{m})\}}{(1 - 2\tilde{m})r_c^2(4 + y)^2[4(1 - 3\tilde{m}) - y(3 - 5\tilde{m})]}$$

$$> 0, \quad (18)$$

Table 1 The BH mass in units of solar masses, the magnetic field B_{SI} in Tesla and the corresponding value of the dimensionless parameter mB. The first two rows are according to (Piotrovich et al. 2010). The orders of magnitude we use in this paper are of 10^{-2} (three following rows), and finally $(mB)_{max} = 0.189366$ could correspond to a ten solar masses BH with a magnetic field of $B_{SI} \approx 10^{16}$ Tesla, or to a more massive BH in a less intense magnetic field

BH mass	B_{SI}	mB
10	10^4	1.4×10^{-11}
10^6	1	1.2×10^{-10}
10^6	10^8	10^{-2}
10^1	10^{13}	10^{-2}
10^4	10^{10}	10^{-2}
10^1	1.6×10^{16}	0.189

where we have used $\tilde{m} = m/r_c$ and $y = B^2 r_c^2$ to compress the expression, and

$$A_0(\tilde{m}) = 64[-6\tilde{m}^2 + \tilde{m}],$$

$$A_1(\tilde{m}) = 672\tilde{m}^2 - 624\tilde{m} + 128,$$

$$A_2(\tilde{m}) = -200\tilde{m}^2 + 204\tilde{m} - 48,$$

$$A_3(\tilde{m}) = 30\tilde{m}^2 - 37\tilde{m} + 12. \tag{19}$$

The denominator in Eq. (18) is positive since $r > 2m$, then the condition for stable orbits, $V''_{eff} > 0$ amounts to the factor in curly brackets being positive,

$$\{y^3 A_3(\tilde{m}) + y^2 A_2(\tilde{m}) + y A_1(\tilde{m}) + A_0(\tilde{m})\} > 0. \tag{20}$$

Moreover, the condition for ISCO is that the previous factor be zero. ISCO are the marginally stable orbits: circular orbits with radius less than the ISCO are unstable and those with radii larger than it are stable. Then the ISCO defines the border of the region of bound orbits, or the inner radius of an accretion disk. For charged and uncharged particles, the ISCO are shown in Fig. 5, fixing the values of κ and L and varying r_c/m and $(mB)^2$. In Fig. 5a) the ISCO for charged particles are shown and in Fig. 5b) for the uncharged particles in the same ranges of r_c/m and $(Bm)^2$. The boundary between the regions represents the ISCO, while the pairs $(r_c/m, (mB)^2)$ corresponding to stable circular orbits (SCO) are in the region below the curve. For fixed L, the available region of SCO is smaller for uncharged particles.

In the next section we establish the relationship between the parameters of the stable circular orbits (orbits obeying $V_{eff}(r_c) = V'_{eff}(r_c) = 0$ and $V''_{eff}(r_c) > 0$) and the redshift of the light emitted by particles traveling along those geodesics.
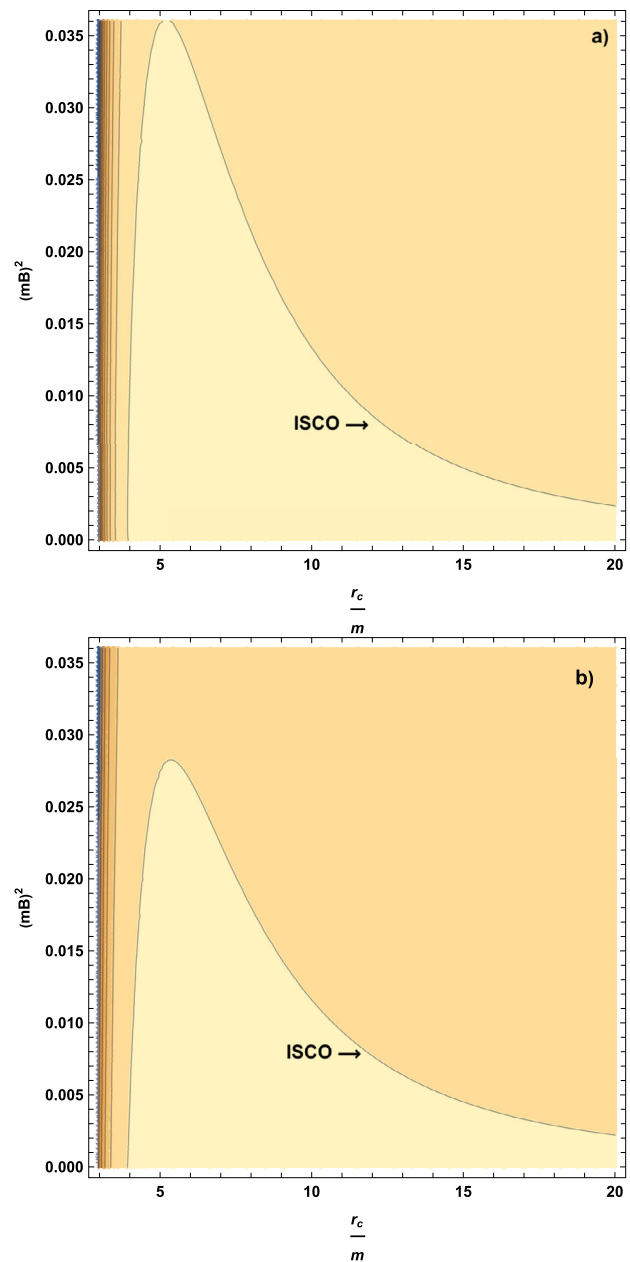

Fig. 5 **a)** The pairs $(r/m, (mB)^2)$ corresponding to ISCO for charged test particles with $\kappa = 0.4$. In **b)** The respective pairs of ISCO for uncharged test particles ($\kappa = 0$) are shown. In both $L/m = 6$. The regions below the ISCO curve are the ones for SCO in each case

3 The red-blueshifts of the photons emitted by particles orbiting the Ernst BH

The connection between the red-blueshifts of the photons emitted by massive particles (stars or gas) that move in stable geodesics around a black hole was pointed out in (Herrera-Aguilar and Nucamendi 2015). Let us start by giving a summary of the method considering a static spacetime (for more details see (Becerril et al. 2016)).

3.1 The red-blueshifts of the photons emitted by charged particles

Light emitted from massive particles moving along stable circular geodesics is characterized by a 4-momentum κ^μ that is a null vector, $\kappa^\mu \kappa_\mu = 0$; photon energy and angular momentum are conserved quantities, $-E_\gamma = g_{tt}\kappa^t$ and $L_\gamma = g_{\phi\phi}\kappa^\phi$, and the photon impact parameter is defined as $b = L_\gamma/E_\gamma = \pm\sqrt{-g_{\phi\phi}/g_{tt}}$.

The frequency shift z associated with the emission (e) and detection (d) of photons emitted from particles in circular geodesics ($U^r = 0$) and equatorial motion ($U^\theta = 0$), is given by

$$1 + z = \frac{U_e^t - b_e U_e^\phi}{U_d^t - b_d U_d^\phi}. \tag{21}$$

Considering that observational redshifts are reported in terms of the kinematic frequency shift, $z_{kin} = z - z_c$, where z_c is the shift of a photon emitted by a static particle at $b = 0$ (on the line going from the center of coordinates) and using the previous Eq. (21), z_c can be written as

$$1 + z_c = \frac{U_e^t}{U_d^t}. \tag{22}$$

For geodesics with $U^r = 0$ and $U^\theta = 0$, in this same context the kinematic frequency shift can be expressed as;

$$z_{kin} = \frac{U_e^t U_d^\phi b_d - U_d^t U_e^\phi b_e}{U_d^t(U_d^t - b_d U_d^\phi)}; \tag{23}$$

if we consider that the detector is located far away from the black hole then from (7) and (23) we obtain

$$z = U_e^\phi b_+ \mid_{r_c} = \sqrt{-\frac{g_{\phi\phi}}{g_{tt}}}\left(\frac{L}{g_{\phi\phi}} - \frac{\kappa A_\phi}{g_{\phi\phi}}\right)\mid_{r_c}. \tag{24}$$

Therefore the redshift z, Eq. (24), of the light emitted by charged particles from a stable circular orbit of radio r_c in the equatorial plane of the Ernst BH is determined by

$$z \mid_{r_c} = \sqrt{\frac{1}{r(r-2m)}}\left(L - \kappa A_\phi\right). \tag{25}$$

Choosing appropriate values of L from the ranges shown in Fig. 4 and from Eq. (11) we determine the behavior of the redshift z for the Ernst BH, as shown in Fig. 6 for different values of κ and varying mB in the range $(0, 0.11)$. The redshift z for the Ernst BH as a function of r_c/m is shown in Fig. 6a); we observe that z decreases as r_c/m augments; the behavior is similar for the photons emitted by neutral particles but the available range of stable orbits is smaller.

In Fig. 6b) the behavior of z of the Ernst BH for different values of the specific charge κ is shown; increasing
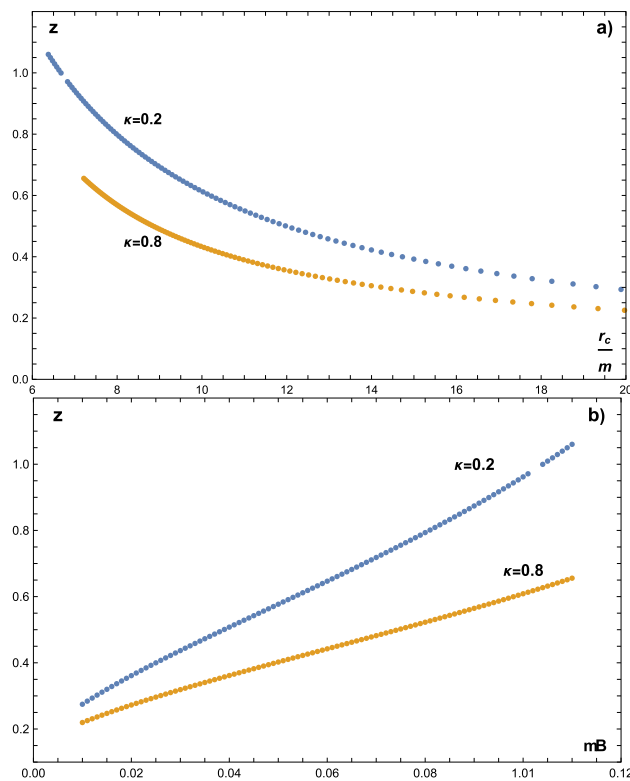

Fig. 6 The redshift of light emitted by charged particles in stable circular orbits of the Ernst BH. **a)** The redshift z as a function of $\frac{r_c}{m}$, and **b)** z as a function of Bm; in both are fixed $L/m = 6$

mB the redshift z increases as well, i.e. the redshift is larger coming from particles in orbits nearer the horizon and z is larger as well for a BH immersed in a magnetic field than for Schwarzschild.

3.2 Redshift from uncharged particles orbiting the Ernst BH

The redshift z of the light emitted by neutral particles in a stable circular orbit of radio r_c in the equatorial plane around the Ernst BH is given by

$$z^2 \mid_{r_c} = \frac{r[m\Lambda + r\Lambda'(r-2m)]}{\Lambda^2(r-2m)[\Lambda(r-3m) - 2r\Lambda'(r-2m)]}, \tag{26}$$

since the radius is always larger than the one of the event horizon, $r > 2m$, then the condition that $z^2 > 0$ reduces to $[\Lambda(r-3m) - 2r\Lambda'(r-2m)] > 0$; this condition reduces to the inequality (17) that we derived from the requirements that $E^2 \geq 0$ and $L^2 \geq 0$. Remember that $r_c > 3m$, i.e. the radius of stable orbits is always greater than $3m$ that is the photosphere radius of Schwarzschild BH. In the case $B \to 0$ we recover the redshift z for Schwarzschild BH (see (Becerril et al. 2016)). From the previous expression we can deter-
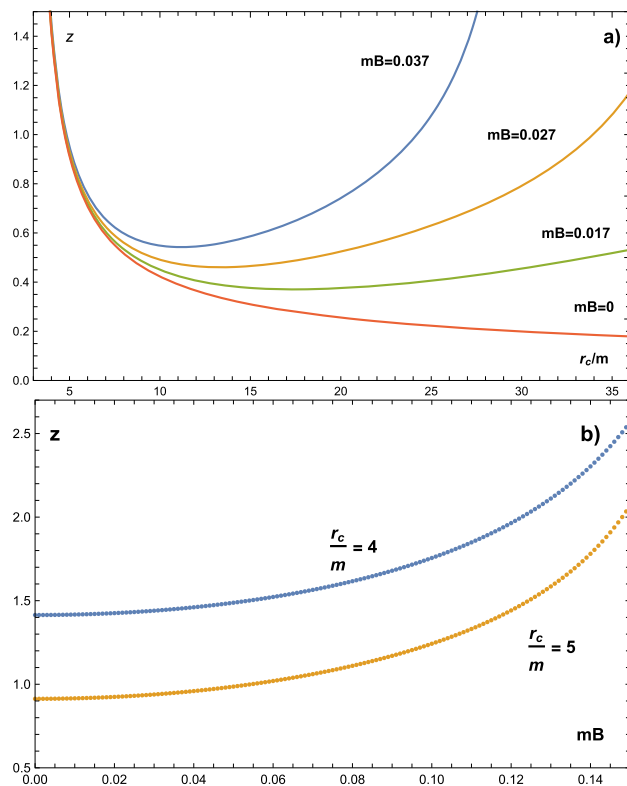
Fig. 7 The redshift of light emitted by neutral particles in SCO around the Ernst BH. **a)** Behavior of z respect to $\frac{r_c}{m}$, for different values of Bm and **b)** the redshift z as a function of Bm, for two values of the radius of the circular orbits from which light is emitted, $\frac{r_c}{m} = 4, 5$. For fixed r_c the presence of the magnetic field increases the redshift

mine $m = r_c \mathcal{G}(z^2, B^2 r_c^2)$ with;

$$\mathcal{G}(z^2, B^2 r_c^2)$$
$$= \frac{-64 + 48y + (4+y)^2(11y - 20)z^2 \pm P(z^2, y)}{4(4+y)^2(5y - 12)z^2},$$
(27)

where $P^2(z^2, y) = 256(4 - 3y)^2 - 32(4 + y)^3(7y - 20)z^2 + (4 + y)^6 z^2$, with $y = B^2 r_c^2$. The redshift z, Eq. (26), of light coming from uncharged particles is shown in Fig. 7 for different values of mB and r_c/m. Figure 7a) shows z as a function of r_c; for $mB \to 0$ the behavior of z is the one of Schwarzschild BH. The redshift z for the Ernst BH decreases as $\frac{r_c}{m}$ augments. For values of $mB > 0.17$ the curve for z presents a minimum and then increases; the ranges for $\frac{r_c}{m}$ are the same as in Fig. 4. It is worth to mention that the Schwarzschild BH redshift is less than the one coming from the Ernst BH $z^S < z^E$, for a given BH mass, so that the effect of the magnetic field is of increasing the redshift but the number of stable orbits is less.

In Fig. 7b) is displayed z as a function of mB for two values of the radius of the circular orbits from which light is

emitted $\frac{r_c}{m} = 4, 5$. For fixed r_c the presence of the magnetic field increases the redshift.

Moreover, from the condition $V''_{\text{eff}}(r_c) = 0$ we obtain a restriction for the ISCO, as a quadratic equation for $\tilde{r}_c = r_c/m$,

$$[30y^3 - 200y^2 + 672y - 384] + [12y^3 - 48y^2 + 128y]\tilde{r}_c^2$$
$$+ [-37y^3 + 204y^2 - 624y + 64]\tilde{r}_c = 0,$$
(28)

here $y = (mB)^2 \tilde{r}_c^2$; the previous Eq. (28), is equivalent to a cubic equation for y,

$$y^3[30 - 37\tilde{r}_c + 12\tilde{r}_c^2] + y^2[-200 + 204\tilde{r}_c - 48\tilde{r}_c^2]$$
$$+ y[672 - 624\tilde{r}_c + 128\tilde{r}_c^2] + 64\tilde{r}_c - 384 = 0.$$
(29)

The 4-velocities of test particle emitters along the stable circular orbits in terms of the BH parameters (m, B) and r_c are

$$(U^\phi)^2 = \frac{(4+y)^2[4m + y(2r_c - 3m)]}{16r_c^2[4(r_c - 3m) - y(3r_c - 5m)]},$$

$$(U^t)^2 = \frac{16r_c(4 - y)}{(4+y)^2[4(r_c - 3m) - y(3r_c - 5m)]},$$
(30)

that impose the restriction on the magnetic field B, that $(4 - y) > 0$ or $B^2 < 4/r_c^2$. The angular velocity of the emitters in these circular geodesics is

$$\Omega^2 = \frac{(4+y)^4[4m + y(2r_c - 3m)]}{256r_c^3(4 - y)},$$
(31)

recalling that $m = r_c \mathcal{G}(z^2, r_c, B^2)$, Eq. (27), indeed these velocities, U^ϕ, U^t, Ω depend on the magnetic field and correspond to a certain redshift z. In such a way that given a set of observables $\{z, r_c\}_i$, Bayesian statistical analysis would provide an estimate for both parameters m and B.

4 Conclusions

In this work we analyze the redshift of the photons emitted by massive and charged test particles that move around a black hole immersed in an external magnetic field, situation represented by the Ernst metric. We consider that the emitters of light are moving along stable circular orbits (SCO). In terms of the effective potential SCO obey that $V'_{\text{eff}}(r_c) = V_{\text{eff}}(r_c) = 0$ and $V''_{\text{eff}}(r_c) > 0$.

The radii of the circular orbits are as well modified in presence of the magnetic field; these radii r_c are shifted towards the horizon in proportion to the magnitude of the magnetic field, i.e. the minima of the effective potential r_c is nearer the horizon as mB augments; or $r_c^E > r_c^S$, i.e. the radius SCO in Schwarzschild BH is less than radius of SCO for the Ernst BH. We obtain numerically the density regions

of the pairs angular momentum-Magnetic fields (L, B) that correspond to SCO of the charged test particles. The set depends on the specific charge of the test particle.

Moreover, we determine the ranges of the parameters that allow the existence of circular orbits of neutral test particles corresponding to SCO. It is also presented the region for the innermost stable circular orbits (ISCO) in terms of the radius of the orbit r_c and the dimensionless parameter mB. We found that there is an upper bound for the magnetic field that allow SCO, $(mB)_{max} = 0.189366$; this field could correspond to a ten solar masses BH with a magnetic field of $B_{SI} \approx 10^{16}$, or to a lesser magnetic field with a more massive BH (see Table 1).

We have shown that the magnetic field affects, through the curvature, neutral or uncharged test particles: the redshift emitted in the presence of the magnetic field is larger than the shift in absence of the field, i.e. light coming from particles orbiting the Schwarzschild BH is less redshifted than the one coming from the BH immersed in a magnetic field.

In summary, the presence of the magnetic field in the vicinity of the BH, considering SCO of neutral and charged particles, enlarges the redshift of the light coming from test particles orbiting the BH. This effect should be taken into account in observations, mainly when strong magnetic field are involved; otherwise it could lead to overestimate the BH mass.

References

Abbott, B.P., et al.: Phys. Rev. Lett. **116**(6), 061102 (2016). https://doi.org/10.1103/PhysRevLett.116.061102. arXiv:1602.03837

Akiyama, K., et al.: Astrophys. J. Lett. **875**, 1 (2019). https://doi.org/10.3847/2041-8213/ab0ec7. arXiv:1906.11238

Aliev, A.N., Ozdemir, N.: Mon. Not. R. Astron. Soc. **336**, 241 (2002). https://doi.org/10.1046/j.1365-8711.2002.05727.x. arXiv:gr-qc/0208025

Becerril, R., Valdez-Alvarado, S., Nucamendi, U.: Phys. Rev. D **94**(12), 124024 (2016). https://doi.org/10.1103/PhysRevD.94.124024. arXiv:1610.01718

Begelman, M.C.: Am. Assoc. Adv. Sci. **300**(5627), 1898 (2003). https://doi.org/10.1126/science.1085334

Breton, N., Lopez, L.A.: Phys. Rev. D **94**(10), 104008 (2016). https://doi.org/10.1103/PhysRevD.94.104008. arXiv:1607.02476

Cardoso, V., Miranda, A.S., Berti, E., Witek, H., Zanchin, V.T.: Phys. Rev. D **79**, 064016 (2009). https://doi.org/10.1103/PhysRevD.79.064016. arXiv:0812.1806

Dadhich, N., Hoenselaers, C., Vishveshwara, C.V.: J. Phys. A, Math. Gen. **12**(2), 215 (1979). https://doi.org/10.1088/0305-4470/12/2/009

Eisenhauer, F., et al.: GRAVITY: Microarcsecond Astrometry and Deep Interferometric Imaging with the VLT p. 361. Springer, Dordrecht (2009)

Ernst, F.J.: J. Math. Phys. **17**(1), 54 (1976). https://doi.org/10.1063/1.522781.

Fernando, S., Correa, J.: Phys. Rev. D **86**, 064039 (2012). https://doi.org/10.1103/PhysRevD.86.064039

Frolov, V.P., Shoom, A.A.: Phys. Rev. D **82**, 084034 (2010). https://doi.org/10.1103/PhysRevD.82.084034. arXiv:1008.2985

Hackstein, J.P., Hackmann, E.: Gen. Relativ. Gravit. **52**(2), 22 (2020). https://doi.org/10.1007/s10714-020-02675-1. arXiv:1911.07645

Herrera-Aguilar, A., Nucamendi, U.: Phys. Rev. D **92**(4), 045024 (2015). https://doi.org/10.1103/PhysRevD.92.045024. arXiv:1506.05182

Konoplya, R.A.: Phys. Lett. B **644**, 219 (2007). https://doi.org/10.1016/j.physletb.2006.11.018. arXiv:gr-qc/0608066

Konoplya, R.A., Fontana, R.D.B.: Phys. Lett. B **659**, 375 (2008). https://doi.org/10.1016/j.physletb.2007.10.065. arXiv:0707.1156

Konoplya, R.A., Stuchlík, Z.: Phys. Lett. B **771**, 597 (2017). https://doi.org/10.1016/j.physletb.2017.06.015. arXiv:1705.05928

Kraniotis, G.V.: Eur. Phys. J. C **81**(2), 147 (2021). https://doi.org/10.1140/epjc/s10052-021-08911-5. arXiv:1912.10320

Lim, Y.-K.: Phys. Rev. D **91**(2), 024048 (2015). https://doi.org/10.1103/PhysRevD.91.024048. arXiv:1502.00722

Lopez, L.A., Hinojosa, V.: Can. J. Phys. **99**(1), 44 (2021). https://doi.org/10.1139/cjp-2019-0572. arXiv:1810.09034

Melvin, M.A.: Phys. Rev. **139**, 225 (1965). https://doi.org/10.1103/PhysRev.139.B225

Piotrovich, M.Y., Silant'ev, N.A., Gnedin, Y.N., Natsvlishvili, T.M.: Magnetic Fields of Black Holes and the Variability Plane (2010). arXiv:1002.4948

Tursunov, A., Stuchlík, Z., Kološ, M.: Phys. Rev. D **93**(8), 084012 (2016). https://doi.org/10.1103/PhysRevD.93.084012. arXiv:1603.07264

Wald, R.M.: Phys. Rev. D **10**, 1680 (1974). https://doi.org/10.1103/PhysRevD.10.1680

Wild, W.J., Kerns, R.M.: Phys. Rev. D **21**, 332 (1980). https://doi.org/10.1103/PhysRevD.21.332